Catalysis Today 155 (2010) 35–44

Contents lists available at ScienceDirect

Catalysis Today

journal homepage: www.elsevier.com/locate/cattod

Technology of methane combustion on granulated catalysts for environmentally friendly gas turbine power plants

Zinfer R. Ismagilov[a,*], Nadezhda V. Shikina[a], Svetlana A. Yashnik[a], Andrei N. Zagoruiko[a], Mikhail A. Kerzhentsev[a], Vladimir A. Ushakov[a], Vladimir A. Sazonov[a], Valentin N. Parmon[a], Vladimir M. Zakharov[b], Boris I. Braynin[b], Oleg N. Favorski[b]

[a] Boreskov Institute of Catalysis, Pr. Ak. Lavrentieva, 5, Novosibirsk 630090, Russia
[b] Central Institute of Aviation Motors, Moscow, Russia

ARTICLE INFO

Article history:
Available online 21 May 2010

Keywords:
Methane catalytic combustion
Gas turbine power plant
Pd–ceria catalyst
Pd–hexaaluminate catalyst

ABSTRACT

The technology of methane combustion in small gas turbine catalytic combustors on alternative granulated catalysts with a low content of noble metals has been developed and studied. The operations of catalyst packages for environmentally clean combustion consisting of one-, two- or three catalysts with different chemical composition, shape and size of granules have been analyzed. The optimized design of a three-stage catalyst package with total height of 340 mm includes 40 mm of highly active Pd–Ce–Al_2O_3 at the entrance of the combustion chamber in the form of 7.5 mm × 7.5 mm × 2.5 mm rings; 240 mm of a basic catalyst based on Mn–hexaaluminate with the granules of the same form and size; and 60 mm of Pd–Mn–La–Al_2O_3 catalyst as 4–5 mm spherical granules at the exit of the combustion chamber. Such optimal design yielded methane combustion over 99.97% at T_{inlet} = 470–580 °C and oxygen excess coefficient 5.2–7.0. The emission levels were NO_x < 1 ppm, CO < 10 ppm, HC < 10 ppm. The pressure drop across the catalyst package was less than 4% of the total pressure (1 bar).

© 2010 Elsevier B.V. All rights reserved.

1. Introduction

Gas turbine power plants (GTPPs) of low power (tens of kW to 1.5–2 MW) are promising autonomous sources of energy and heat. The application of gas turbine technologies saves fuel, solves heat supply and water shortage problems. The nominal efficiency of GTTPs belonging to different generations varies from 24% to 38% (average weighted efficiency – 29.0%). This is 1.5 times higher than that of combined heat power plants.

The main GTPP drawback is significant emission of toxic nitrogen oxides due to high-temperature combustion of the gas fuel. The main approach used today to decrease the emission of nitrogen oxides from GTPPs is based on the use of the so-called homogeneous combustion chambers. They are based on feeding specially prepared fuel–air mixture with 2-fold excess of air ("lean" fuel–air mixture). This technology makes it possible to decrease significantly the temperature in the combustion zone relative to traditional GTPP combustion chambers with separate supply of fuel and air to the combustion zone. As a result, the concentration of nitrogen oxides in the flue gases decreases from 100 to 10–20 ppm.

However, the most efficient way to decrease emissions of nitrogen oxides in GTPPs is to use catalytic combustion of fuel [1–4]. In the catalytic chamber efficient combustion of homogeneous fuel–air mixture is achieved at larger excess of air and much lower temperatures in the zone of chemical reactions compared to modern homogeneous combustion chambers.

In the last decade, the obvious advantages of the catalytic chambers in GTPPs initiated intense scientific and applied studies in the USA (Catalytica) and Japan (Kawasaki Heavy Industries) which are aimed at development of such chambers for GTPPs for various applications [5–8].

Today catalysts for gas turbines are prepared in the form of monoliths from foil made of special corrosion-resistant alloys with deposited porous support and the active component based on platinum and/or palladium [5,9,10]. However, application of such catalysts requires many problems to be solved. The main problems are related to the high temperature of gas typical for modern gas turbines that requires the catalyst to operate at temperatures exceeding 1200 K for prolonged periods of time (total operation time of modern GTPPs reaches 100,000 h) [11]. The use of metal supports at temperatures above 900 °C is limited due to possible thermal corrosion, especially in the presence of water vapor. It results in the catalyst destruction, peeling of the support and loss of noble metals decreasing the catalytic activity and shortening the

* Corresponding author. Tel.: +7 383 3306219; fax: +7 383 3306219.
E-mail address: zri@catalysis.ru (Z.R. Ismagilov).

0920-5861/$ – see front matter © 2010 Elsevier B.V. All rights reserved.
doi:10.1016/j.cattod.2010.04.008

catalyst lifetime. So, the improvement of the catalyst stability is an urgent problem to be solved.

One of the approaches to solve this problem is based on the development of catalysts on granulated supports and design of a catalytic package for GTPP combustion chamber, which would have good ecological parameters at moderate temperatures (930–950 °C). We developed granulated oxide catalysts $Mn–Al_2O_3$ [12,13], $Mn–La–Al_2O_3$ [12–14,16] and palladium catalysts with low palladium concentrations $Pd–CeO_2–Al_2O_3$ [14,15] and $Pd–Mn–La–Al_2O_3$ [16]. It is important that the active component phases in the catalysts are formed at high temperatures – 900–1000 °C. Earlier we studied the catalytic properties of these catalysts in methane oxidation and their thermal stability up to 1000 °C as a function of preparation method, phase composition of the support, precursors, active component concentration and calcination temperature. The catalyst preparation method was optimized based on the obtained results. Pilot batches of several catalysts were synthesized: Mn/Al_2O_3 - ICT-12-40A, $Mn–La–Al_2O_3$ - IC-12-61, $Pd/Ce/Al_2O_3$ - IC-12-60, and $Pd–Mn–La–Al_2O_3$ - IC-12-62. The batches were tested in a model experimental installation reproducing with reasonable precision the operating conditions of the catalysts in gas turbine power plants in all process parameters, except for the pressure in the GTPP combustion chamber. The preliminary tests in the model GTPP combustion chamber showed that methane combustion with good emission characteristics was possible using the developed catalysts [17].

This study was devoted to the design of a catalytic package providing low emissions of NO_x, CO and HC under testing conditions simulating the operation conditions of a catalytic combustion chamber in a low-power (300–600 kW) GTPP with regeneration cycle. The paper reports the results of tests carried out in the catalytic combustion chamber (CCC) of a pilot testing installation with varied composition of the catalytic package and testing conditions and mathematical simulation of the catalytic combustion processes in the catalytic combustion chamber. A catalytic package design optimized on the basis of the experimental studies is suggested.

2. Experimental

2.1. Catalyst preparation

Pilot batches of the following catalysts: Mn/Al_2O_3 - ICT-12-40A, $Mn–La–Al_2O_3$ - IC-12-61, $Pd–Ce–Al_2O_3$ - IC-12-60, and $Pd–Mn–La–Al_2O_3$ - IC-12-62 were synthesized according to the earlier reported procedures [15]. Their main physicochemical and catalytic properties are given in Table 1.

2.2. Catalyst characterization

The textural properties of the samples (specific surface area, S_{BET} (m^2/g); pore volume V_{meso} (cm^3/g)) were studied by adsorption methods using ASAP-2400 instrument. The total pore volume (V_Σ, cm^3/g) was estimated from incipient wetness.

The phase composition of the samples was studied by XRD using HZG-4 diffractometer with monochromatic Co Kα irradiation. The ICPDS XRD database was used for the phase identification.

The mechanical crushing strength of the samples (P, kg/cm^2) was measured using MP-9C instrument designed for determination of the strength of porous solids under static conditions.

2.3. Catalytic activity tests

The catalysts were tested in methane combustion using a laboratory installation and in combustion of natural gas using a CCC of a pilot test installation.

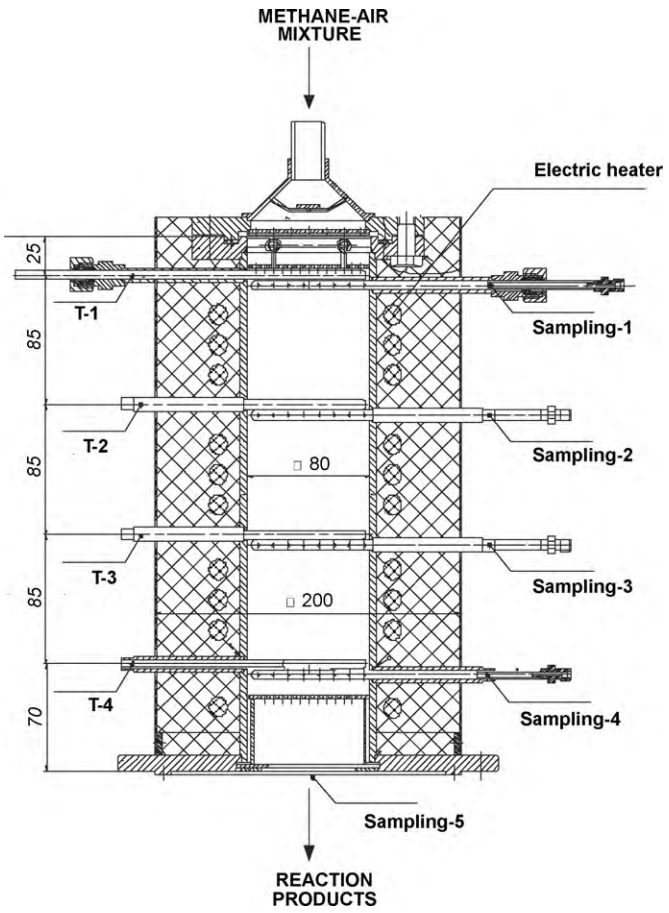

Fig. 1. Schematic view of a catalytic combustion chamber: T-1 to T-4: thermocouples, sampling 1–5: samplers.

The catalyst tests in methane oxidation in the laboratory installation were carried out using a quartz flow reactor, 0.5–1.0 mm catalyst fraction at GHSV = 1000–48,000 h^{-1} and gas phase composition 1 vol.% CH_4 in air. The coefficient of oxygen excess over the stoichiometric value (α) was 10.4. It was calculated using Eq. (1):

$$\alpha = \frac{(100 - C_{CH_4}) \times 0.21}{2C_{CH_4}} \quad (1)$$

Here C_{CH_4} is the methane concentration in the feed (vol.%), 0.21 is the volume fraction of O_2 in air, 2 is the stoichiometric coefficient for O_2 according to Eq. (2):

$$CH_4 + 2O_2 = CO_2 + 2H_2O \quad (2)$$

The reaction products were analyzed by gas chromatography. The CH_4 conversion (X_{CH_4}) was calculated from the experimental concentrations of the reagents and products using Eq. (3):

$$X_{CH_4} = \frac{C^0_{CH_4} - C_{CH_4}}{C^0_{CH_4}} \times 100\% \quad (3)$$

Here $C^0_{CH_4}$ and C_{CH_4} are methane concentrations (vol.%) in the feed and reaction products, respectively. The experimental data were presented as dependences of methane conversion on temperature.

The catalysts tests in CCC was carried out in a stainless-steel tubular vertical reactor with internal diameter Ø = 80 mm. The CCC is schematically shown in Fig. 1. The volume of the catalytic package was 1.3 L.

In the experiments, natural gas containing 97 vol.% methane, 2 vol.% ethane and 0.5 vol.% nitrogen and carbon dioxide was used.

Table 1
Physicochemical properties of the catalysts before and after CCC tests.

Catalyst	T_{cal} (°C)	Physicochemical and catalytic properties					
		Chem. compos. wt.%	XRD phase composition	S_{BET} (m^2/g)	V_{meso}/V_{Σ} (cm^3/g)	P (kg/cm^2)	$T_{50\%\ CH_4}$, (°C)
Pd–Ce–Al_2O_3 - IC-12-60 rings, initial	1000	Pd – 2.1 Ce – 10.1	δ-Al_2O_3 CeO_2 (D[a] ~ 200 Å, S_{33} = 1100)[b] PdO (D ~ 180 and 250 Å, S_{39} = 480)	74	0.25/0.37	22	330
After 72 h tests at T_{in} – 470 °C			(δ + γ)-Al_2O_3 CeO_2 (D ~ 200 Å, S_{33} = 1100) PdO(D > 170 Å, S_{39} = 480)	68	0.28/0.40	25	290
Mn-Al_2O_3 - ICT-12-40A rings, initial	900	Mn – 6.9	(δ + γ)-Al_2O_3 α-Al_2O_3 Mn_2O_3	80	0.23/0.40	23	400
After 80 h tests at T_{in} – 600 °C			α-Al_2O_3 Mn_2O_3 (Mn, Al)Al_2O_4[c]	10	0.01/0.38	12	460
Mn–La–Al_2O_3 - IC-12-61 rings, initial	1000	Mn – 6.9 La – 10.1	γ*-Al_2O_3 (a = 7.925 Å) $MnLaAl_{11}O_{19}$ (S_{37} = tr)	43	0.23/0.33	34	420
After 72 h tests at T_{in} – 600 °C			γ*-Al_2O_3 (a = 7.942 Å) Disorderd $MnLaAl_{11}O_{19}$ (S_{37} = tr)	32	0.21/0.35	27	420
Pd–Mn–La–Al_2O_3 - IC-12-62 rings, initial	1000	Pd – 0.65 Mn – 7.1 La – 9.4	$MnLaAl_{11}O_{19}$ (S_{37} = tr) γ*-Al_2O_3 (a = 7.937 Å) PdO (D ~ 300 Å, S_{39} = 70)	46	0.21/0.36	25	385
After 124 h tests at T_{in} – 575 °C			$MnLaAl_{11}O_{19}$ (S_{37} = tr) γ*-Al_2O_3 (a = 7.937 Å) γ*-Al_2O_3 (a = 7.942 Å)	36	0.21/0.36	27	340
Pd–Mn–La–Al_2O_3 - IC-12-62 spheres, initial	1000	Pd – 0.5 Mn – 6.1 La – 10.2	$MnLaAl_{11}O_{19}$ (S_{37} = tr) γ*-Al_2O_3 (a = 7.925 Å) PdO (D < 150 Å)	50	0.24/0.30	70	380
After 50 h tests			$MnLaAl_{11}O_{19}$ (S_{37} = tr) γ*-Al_2O_3 (a = 7.937 Å) α-Al_2O_3	37	0.24/0.30	95	350

[a] Particle size was determined from the coherent scattering area.
[b] Relative concentrations of phases present in the samples were determined from the areas of peaks in the diffraction pattern in arbitrary units.
[c] Solid solution based on (Mn, Al)Al_2O_4 spinel, γ*-Al_2O_3: a solid solution based on γ-Al_2O_3.

The air excess coefficient (α) was selected to be close to the minimum value of this parameter in the operating regime of full-power GTPP CCC (α = 6.4–6.8). The inlet temperature of the fuel–air mixture T_0 was varied between 470 and 600 °C, the temperature at the chamber exit T_{ex} was 900–985 °C, the GHSV of the fuel–air mixture was 8500–15,000 h^{-1}.

Natural gas was introduced into the combustion chamber after reaching the light-off temperature. Due to the natural gas combustion, the temperature in the catalyst bed increased and reached the values close to the desired ones in 30–40 min. The temperature mode was corrected by smooth variation of the air and natural gas flows.

When the desired temperature regime was reached, temperatures along the length of the catalytic chamber were measured. The radial temperature profile was measured before and after the pilot-plant tests. A reference manometer was used to measure the pressures in the catalyst bed. The gas phase composition at the CCC outlet was analyzed using a "Kristall-2000 M" gas chromatograph. The gas probes were also analyzed in parallel using ECOM-AC gas analyzer.

2.4. Mathematical model analysis

For the methane oxidation reaction we assumed that only deep oxidation to CO_2 and H_2O takes place in the oxygen excess. The reaction rate was calculated using Eq. (4):

$$W = k_0(1-\varepsilon)\exp\left(-\frac{E/R}{T}\right) C_{CH_4}\left(\frac{P}{P_0}\right) \quad (4)$$

Here k_0 is the pre-exponential factor of the kinetic constant (s^{-1}), E is the activation energy (J/mol), R is the universal gas constant (J mol^{-1} K^{-1}), ε is the fractional void volume in the catalyst bed, C_{CH_4} is the methane concentration (molar fraction), P is the operating pressure (atm), P_0 is the basis pressure (bar) at which the reaction kinetics was studied experimentally, here it is equal to 1 bar.

Table 2
Kinetic parameters (see Eq. (4)) for methane combustion reaction for different catalysts.

Catalyst	k_o (s^{-1})	E (kJ/mol)
Pd–Ce–Al_2O_3	4.36×10^7	81.4
Mn–Al_2O_3	1.09×10^5	71.2
Mn–La–Al_2O_3	1.09×10^5	71.2
Pd–Mn–La–Al_2O_3	3.29×10^5	63.8

The values of kinetic parameters (k_0 and E) determined earlier in kinetic experiments over these catalysts [15] (see Table 2) were used in the calculations.

A heat and mass steady-state model of an ideal displacement adiabatic reactor was used in the simulations of the catalyst bed:

$$u\frac{\partial C_{CH_4}}{\partial \ell} = -W = \beta(C^*_{CH_4} - C_{CH_4}) \quad (5)$$

$$u\frac{\partial T_G}{\partial \ell} = xC^{in}_{CH_4}\Delta T_{AD} = \frac{\alpha_{HE}}{c_p}(T_C - T_G) \quad (6)$$

$$\ell = 0 \Rightarrow C_i = C_i^{in};\ \ T = T_{in} \quad (7)$$

Here u is the linear gas flow rate in the reactor reduced to standard conditions and full reactor cross-section area (m/s), l is the coordinate along the reactor height (m), x is the methane conversion, C^* and C are methane concentrations at the surface of the catalyst grain and in the gas flow, respectively, β is the mass exchange coefficient for methane (s^{-1}), T_G and T_C are gas and catalyst temperatures (K), correspondingly, ΔT_{AD} is the adiabatic heating of the reaction (K), α_{HE} is the heat exchange coefficient (W m^{-3} K^{-1}), c_p

is the gas thermal capacity (J m^{-3} K^{-1}), index *in* corresponds to the conditions at the reactor inlet.

The reaction rate in the kinetic region was determined using Eq. (4) taking into account the kinetic parameters described above. Internal and external diffusion limitations were taken into account during calculation of the apparent reaction rate. Due to the oxygen excess the limitations were considered only for methane diffusion.

The internal diffusion limitation was taken into account using the Thiele modulus approach for the first-order reaction. It is known [18] that the efficiency factor of the catalyst grain η can be found using Eq. (8):

$$\eta = \frac{3}{\varphi}\left(cth\varphi - \frac{1}{\varphi}\right) \tag{8}$$

The Thiele modulus φ, characterizing the influence of the internal diffusion limitations, can be determined using Eq. (9):

$$\varphi = \frac{r}{3}\sqrt{\frac{K}{D_{eff}}} \tag{9}$$

Here r is the equivalent radius of the catalyst grain (m), K is the reaction rate constant in the kinetic region (s^{-1}), D_{eff} is the effective methane diffusion coefficient in the catalyst pores (m^2/s). The effective diffusion coefficient was calculated using Eq. (10) [18]:

$$D_{eff} = \Pi\left(\frac{1}{(1/D)+(1/D_K)}\right) \tag{10}$$

Here Π is the permeability coefficient that was taken as 0.2 [18], D and D_K are the coefficients of molecular and Knudsen diffusion of methane calculated using Eqs. (11) [19] and (12) [18]:

$$D = \frac{4.3\times10^{-7}T_C^{3/2}}{P\left(v_{CH_4}^{1/3}+v_{N_2}^{1/3}\right)^2}\sqrt{\frac{1}{M_{CH_4}}+\frac{1}{M_{N_2}}}\ (m^2/s) \tag{11}$$

$$D_K = 97 r_p\sqrt{\frac{T_C}{M_{CH_4}}}\ (m^2/s) \tag{12}$$

Here v is specific molar volume of methane and nitrogen, which is the main component of the gas mixture (cm^3/atom), M is the molecular mass of methane and nitrogen (carbon units), r_p is the average catalyst pore radius (m). For this catalyst the average pore radius was determined by mercury porosimetry and was equal to 170 Å.

To describe the apparent reaction rate taking into account the external diffusion limitations we used the apparent rate constant k' calculated for pseudo-first reaction order:

$$k\prime = \frac{1}{(1/\eta K)+(1/\beta)} \tag{13}$$

Here β is the mass exchange coefficient for methane (s^{-1}) determined from known criteria equations [20]:

$$\beta = \frac{ShDS_{sp}P}{d_{eq}} \tag{14}$$

$$Sh = ARe^B Sc^{0.33} \tag{15}$$

$$Re = \frac{u_r d_{eq}\rho}{\mu} \tag{16}$$

$$Sc = \frac{\mu\rho}{D} \tag{17}$$

Here *Sh*, *Re*, *Sc* are dimensionless Sherwood, Reynolds and Schmidt criteria, respectively, D is the coefficient of methane molecular diffusion in air (m^2/s), S_{sp} is the specific surface area of the catalyst granules in unit volume of the catalyst bed (m^{-1}), d_{eq} is the equivalent (hydraulic) diameter of the pass in the bed (m), u_r is the actual linear gas flow rate in the bed (m/s), ρ is the gas density (kg/m^3), μ is the gas viscosity (N s m^{-2}).

The actual gas flow rate u_r was calculated with corrections for temperature, pressure and porosity of the catalyst bed:

$$u_r = u\frac{T_G}{273}\frac{1}{\varepsilon}\frac{1}{P} \tag{18}$$

The heat exchange coefficient was calculated similarly:

$$\alpha_{HE} = \frac{Nu\lambda S_{sp}}{d_{eq}} \tag{19}$$

$$Nu = ARe^B Pr^{0.33} \tag{20}$$

Here *Nu* and *Pr* are Nusselt and Prandtl criteria, correspondingly, λ is the thermal conductivity of the reaction gas.

Empirical parameters A and B in Eqs. (15) and (20) were chosen based on the literature recommendations [20] depending on the type of the hydraulic regime. The modified values of the parameters for Eq. (20) providing the cumulative account for both the heat exchange between gas and catalyst and the effective heat conductivity of the catalyst bed [20] were used.

The pressure drop in the catalyst bed was calculated using Eq. (21).

$$\Delta P = \xi\frac{L}{d_{eq}}\frac{\rho u_r^2}{2} \tag{21}$$

Here L is the total height of the catalyst bed (m). The resistance coefficient ξ was calculated using Eq. (22):

$$\xi = \frac{F}{Re^p} \tag{22}$$

where parameters F and p were selected depending on the Reynolds number value (e.g., F = 16.5 and p = 0.2 for turbulent regime at Re > 400).

3. Results and discussion

3.1. Physicochemical properties of the catalysts

The composition, calcination temperature, physicochemical properties (specific surface area S_{BET} (m^2/g), volume of mesopores V_{meso} (cm^3/g), total pore volume V_Σ (cm^3/g), and mechanical crushing strength P (kg/cm^2) and catalytic properties (temperature of 50% methane conversion $T_{50\%\ CH_4}$, (°C), are reported in Table 1.

The investigation of the physicochemical properties of the initial catalyst samples showed that the active component in the initial Pd–Ce–Al_2O_3 was in the form of finely dispersed PdO. This active form initiates combustion of the methane–air mixture at low temperatures. In the Mn/Al_2O_3 catalyst the active phase considered to be Mn_2O_3 initially was converted to a solid solution (Mn, Al)Al_2O_4 with the spinel structure after prolonged thermal treatment at 900 °C. This conversion results from the interaction of Mn_2O_3 with γ-Al_2O_3. This phase is stable up to 1000 °C [21]. The initial catalysts based on Mn and La oxides were characterized by crystallized hexaaluminate phase which is known to be stable at high temperatures [16,22,23]. All the catalysts had average specific surface areas (50–95 m^2/g), pore volumes (0.3–0.4 cm^3/g) and mechanical strengths sufficient for use in high-temperature methane combustion process.

3.2. Tests of CCC with uniform catalyst package

First we tested CCC loaded with one catalyst. Such loading will be hereafter denoted as "uniform" and provides for one-stage combustion of the natural gas–air mixture. Such experiments allowed us to analyze the perspectives of using manganese–alumina catalysts and evaluate their catalytic properties in natural gas combustion by such parameters as outlet temperature and emission of

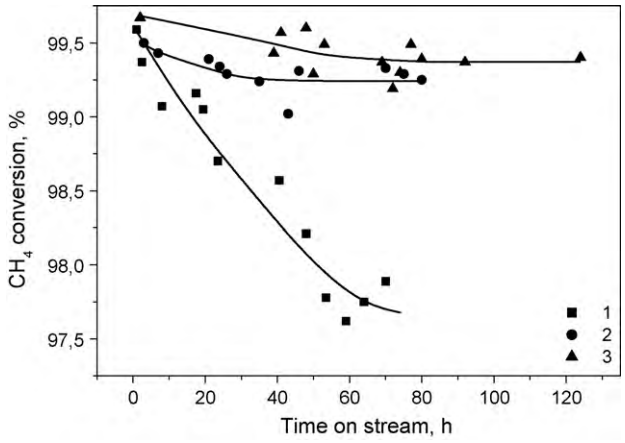

Fig. 2. Methane conversion vs. operation time in CCC at GHSV: 14,900–15,100 h^{-1} and α: 6.7–6.8. Uniform catalyst package loaded with: (1) Mn–Al_2O_3 (T_{in} – 600 °C); (2) Mn–La–Al_2O_3 (T_{in} – 600 °C); (3) Pd–Mn–La–Al_2O_3 (T_{in} – 575–580 °C).

hydrocarbons. Mn–Al_2O_3, Mn–La–Al_2O_3 and Pd–Mn–La–Al_2O_3 catalysts shaped as rings were tested for 72–120 h in a temperature cycle mode. The temperature cycle mode consisted of four cycles of gas combustion, catalyst cooling and repeated start of the combustion process. The combustion process was carried out at GHSV = 15,000 h^{-1} and inlet temperature 580–600 °C. The value of α was maintained at 6.8–6.9. The height of the catalytic package was 300 mm. The dynamics of changes in the activity of different catalysts are presented in Fig. 2.

The data presented in Fig. 2 indicate that the catalysts Mn–Al_2O_3, Mn–La–Al_2O_3 and Pd–Mn–La–Al_2O_3 differ both by their activity and stability. For example, the activity of the Mn–Al_2O_3 catalyst gradually decreased as evidenced by gradual increase of the methane and CO concentration at the CCC outlet. The methane conversion degree decreased from 99.6% to 97.9% during the first 50–54 h on stream. Then the catalyst activity stabilized and did not change in the following 80 h on stream (Fig. 2, curve 1). At the end of the experiment the methane and CO concentrations stabilized at 330 and 110 ppm, respectively (Table 3).

Table 3 compares the outlet temperatures and emissions of CH_4 and CO during natural gas combustion over Mn–Al_2O_3 catalysts with different fractional compositions at GHSV = 8500–15,000 h^{-1}. It was shown that the methane combustion efficiency over large catalyst granules with the external ring diameter 15 mm was low. Even at a low load on the catalyst (GHSV = 8500 h^{-1}) the methane conversion was 97% whereas the methane and CO emissions at the outlet were 500 and 300 ppm, respectively. Note that under similar CCC operation conditions the application of catalyst granules with the external diameter 7.5 mm allowed for a 10-fold decrease of the methane emission and 30-fold decrease of the CO emission. In both cases the CCC efficiency also depended on contact time. The contact time increase from 0.24 s (GHSV = 15,000 h^{-1}) to 0.42 s (GHSV = 8500 h^{-1}) affected more significantly the efficiency of CCC loaded with the catalyst with smaller internal and external diameters of the granules (7.5 mm), i.e. lower fractional void volume of the catalyst bed. These data indicate that the mass transfer of the reagents and reaction products to/from the catalyst surface substantially affects the total CCC efficiency in methane combustion at the inlet temperature 600 °C. At this temperature methane oxidation proceeds mainly on the catalyst surface and the contribution of homogeneous reactions is negligible, which is confirmed by substantial improvement of methane conversion with the increase of the catalysts geometrical surface. These data agree with the work [24] where the authors showed the dependences of relative contributions of heterogeneous and homogeneous methane oxidation

Table 3
Parameters of methane combustion over Mn–Al_2O_3 catalysts with different fractional compositions.

Fraction	G_{air} (m^3/h)	G_{NG} (l/h)	GHSV (h^{-1})	α	T_{inlet} (°C)	T_1[a] (°C)	T_2[a] (°C)	T_3[a] (°C)	T_4[a] (°C)	C_{CH_4} (ppm)	C_{CO} (ppm)	NO_x (ppm)	X_{CH_4} (%)
7.5	19.4	309	14,900	6.78	577	659	867	920	917	328	102	1	97.89
7.5	15.0	243	11,500	6.70	567	677	903	926	905	164	41	2	98.68
7.5	11.1	180	8500	6.67	571	728	923	925	896	48	9	1	99.69
15	19.2	324	14,800	6.41	590	623	763	898	918	987	943	1	93.87
15	15.0	267	11,500	6.10	570	604	783	909	919	630	616	2	96.28
15	11.1	204	8500	5.90	562	591	790	903	897	504	344	2	97.13

[a] Thermocouple places along the catalyst bed at different distances from the CCC inlet: T_1 – 25 mm; T_2 – 110 mm; T_3 – 195 mm; T_4 – 280 mm.

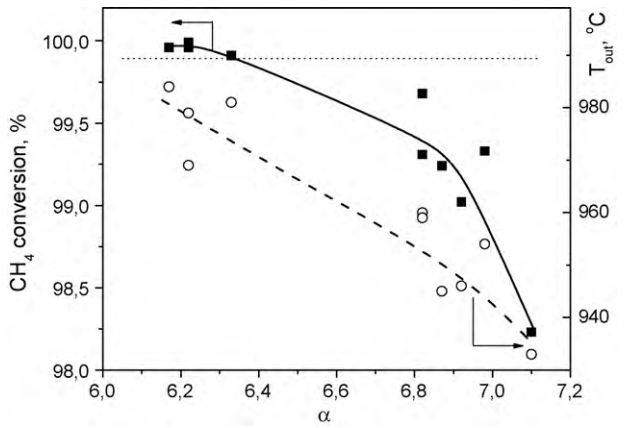

Fig. 3. Dependence of methane conversion (filled symbols) and catalyst temperature at the CCC outlet (open symbols) during methane combustion in CCC loaded with Mn–La–Al_2O_3 catalyst on α. GHSV = 15,000 h^{-1}, T_{in} = 600 °C.

reactions on the monolithic Pt–Pd catalyst on the inlet temperature, pressure and the catalyst channel density. Placing the catalysts with small cells (200 cpsi) in the front part of the reactor allowed the increase of heat release there at 600 °C [24], at the same time in the monolith with larger channels (100 cpsi), especially at temperature 700 °C the homogeneous oxidation reaction was prevailing.

The activity of Mn–La–Al_2O_3 and Pd–Mn–La–Al_2O_3 catalysts also decreased in the first 30–40 h on stream. However, the activity decrease was less dramatic compared to the Mn–Al_2O_3 catalyst (Fig. 2). The methane conversion over Mn–La–Al_2O_3 and Pd–Mn–La–Al_2O_3 catalysts decreased from 99.5% to 99.3% (Fig. 2, curve 2) and from 99.7% to 99.4% (Fig. 2, curve 3), respectively. The concentrations of methane and CO stabilized at 100 and 85 ppm, correspondingly. Note that the Pd–Mn–La–Al_2O_3 catalyst showed these values of the residual CH_4 and CO concentrations at a lower inlet temperature 575 °C than the Mn–La–Al_2O_3 catalyst that showed similar values at 600 °C inlet temperature. The NO_x concentration at the outlet of the catalyst package did not exceed 0–2 ppm on all the catalysts. Thus, the obtained results demonstrate that the activity of the Pd–Mn–La–Al_2O_3 catalyst was higher than that of the catalysts without Pd. Meanwhile, the stability of this catalyst was comparable to that of Mn–La–Al_2O_3 being determined by the Mn–hexaaluminate phase. The stability of these catalysts was much higher than that of the catalyst based on Mn oxide. These results of the catalysts testing under the above conditions are in good agreement with our results on the study of the catalysts activity in methane oxidation in a laboratory reactor [12–14,16]. It was shown that modification of Mn-alumina catalysts with oxides of rare earth metals allowed a considerable increase of thermal stability of the catalysts due to the formation of manganese–hexaaluminate phase [12,16]. Introduction of 0.5 wt.% Pd into Mn–La–Al_2O_3 resulted in a substantial decrease of the light-off temperature of the air–natural gas mixture [16].

The pressure drop on the full height of the catalyst bed for uniform loading of the catalysts in the form of 7.5 mm × 7.5 mm × 2.5 mm rings for the catalysts Mn–Al_2O_3, Mn–La–Al_2O_3 and Pd–Mn–La–Al_2O_3 was 35, 23 and 14 mbar at GHSV = 14,900, 11,500 and 8500 h^{-1}, respectively. These values are less 4% of the total pressure which was 1 bar.

Fig. 3 shows the effect of the oxygen excess coefficient on the outlet temperature and methane conversion over the catalyst package loaded with the Mn–La–Al_2O_3 catalyst. The variation of α between 6.2 and 7.2 showed that its decrease (enrichment of the fuel–air mixture with methane) resulted in a growth of the temperature at the outlet of the catalyst bed and, consequently, increase of the methane conversion. For instance, when α was decreased from 7 to 6.2, the methane conversion increased from 99.3% to 99.93% and the temperature grew from 937 to 992 °C at GHSV = 15,000 h^{-1}. However, Fig. 3 shows that methane conversion above 99.9% was observed when the temperature in the catalyst bed exceeded 980 °C. So high temperature is undesirable because the catalyst overheating during prolonged operation will inevitably lead to its deactivation. Therefore, alternative methods of increasing the methane conversion degree are required.

As it is known from the literature, one of the ways to increase the CCC efficiency is to use multistage (multizone) combustion. This method allows one to control the temperature profile by varying the catalyst activity in different zones of the catalytic combustion chamber. Several methods for stepwise combustion of hydrocarbon fuels in the GTPP CCC have been implemented.

American companies Catalytica [25] and Westinghouse Electric Corp. [26] suggested feeding the fuel–air mixture to a monolith catalyst consisting of alternating channels with an active component and without it. If the surface reaction in the channel with a catalyst takes place in the diffusion-controlled regime, adiabatic heating to the flame temperature does not occur because the heat is transferred to the inert channel of the monolith. The fuel–air mixture exiting the inert channels is burnt at the exit of the monolith catalyst.

In patents [25,27] it was suggested to use multisection catalysts with different levels of activity to carry out combustion in the kinetically controlled regime. The catalytic activity is regulated by varying the concentration of the noble metal (most often Pd) in the range of 5–20 wt.% or the nature of the active component (noble metal, transition metal oxides). It was also suggested [8] to use a two-stage monolithic catalyst combined from catalytic systems with different thermal stabilities. A catalyst with low ignition temperature requiring minimal heating is placed at the entrance zone whereas a catalyst resistant to the action of high temperatures is placed at the exit.

3.3. Tests of CCC with combined two-stage catalyst package

We suggested a design of a two-stage catalyst package consisting of catalysts with the same chemical composition but different fractional compositions. Using the Pd–Mn–La–Al_2O_3 catalyst as an example we studied the effect of the catalyst bed fractional void volume on the methane conversion degree in CCC. The main part of the catalyst package was loaded with the catalyst formed as 7.5 mm × 7.5 mm × 2.5 mm rings having the fractional void volume (ε) 0.52. A catalyst layer with 60 mm height consisting of 4–5 mm spherical granules with fractional void volume 0.42 was placed near the outlet of the package. The total Pd concentration in the catalyst package was 0.6 wt.%.

The application of the spherical catalyst at the CCC outlet made it possible to achieve over 99.9% combustion efficiency (Fig. 4) and decrease the methane concentration from 85 ppm to 0–5 mm and the CO concentration to 4–8 ppm at inlet temperature 580 °C and α in the range of 6.7–7.1. Fig. 5 presents the methane and CO profiles along the reactor length. One can see that more than 90% of methane is oxidized at the distance ca. 200 mm from the inlet. The maximum CO concentration is observed in this region. Further combustion of methane and CO to concentrations below 10 ppm is observed mostly at 280–340 mm from the inlet of the catalyst package, i.e. in the area where the spherical catalyst is loaded. The layer of this catalyst has a higher density and higher geometrical area, which provides more efficient use of the catalyst, and thus increases the CCC efficiency.

Then, we determined the role of catalyst activity in the total CCC efficiency. We carried out tests on a combined catalyst package consisting on Mn–La–Al_2O_3 (rings) and Pd–Mn–La–Al_2O_3 (spheres) and compared the methane conversion with the results of the pre-

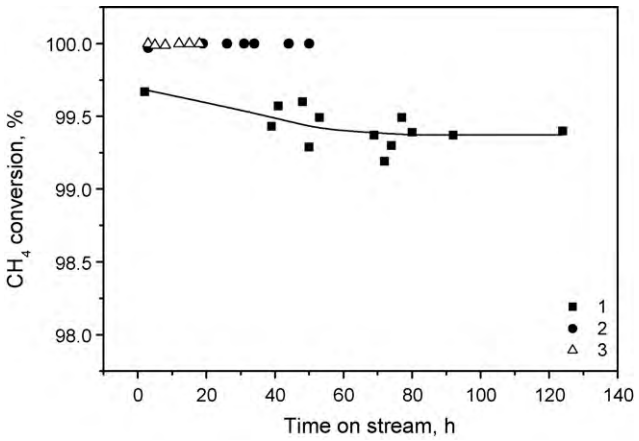

Fig. 4. Methane conversion vs. operation time in CCC for different catalyst packages: (1) uniform catalyst package Pd–Mn–La–Al_2O_3, rings (T_{in} = 575–580 °C, GHSV = 15,100 h^{-1}, α = 6.8–6.9); (2) combined catalyst package: Pd–Mn–La–Al_2O_3, rings and spheres (T_{in} = 575–580 °C, GHSV = 12,500 h^{-1}, α = 6.7–6.8); (3) combined catalyst package: Mn–La–Al_2O_3, rings, and Pd–Mn–La–Al_2O_3, spheres (T_{in} – 575–580 °C, GHSV = 12,500 h^{-1}, α = 6.7–6.8).

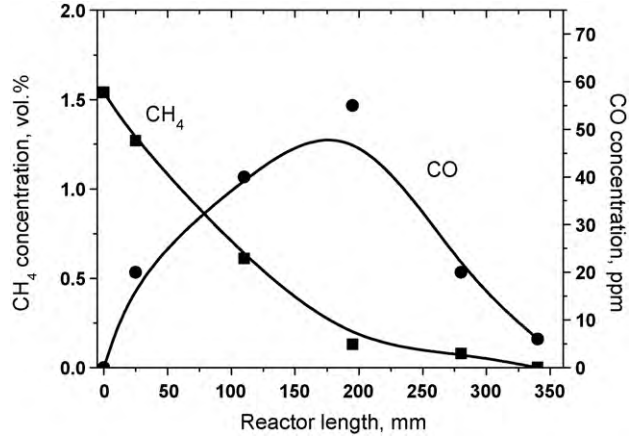

Fig. 5. Profiles of methane and CO concentrations along the reactor length during combustion of natural gas on a combined catalyst package Pd–Mn–La–Al_2O_3: 280 mm of rings and 60 mm of spherical granules (T_{in} = 580 °C, GHSV = 12,500 h^{-1}).

vious test. The ratio of the layer heights was similar to that used in the previous test – 280/60 mm. The total Pd content in CCC was much lower about 0.1 wt.% because most of the catalyst package consisted of the Mn–La–Al_2O_3 catalyst. The activity of this catalyst ($T_{50\%\ CH_4}$) is lower than that of Pd–Mn–La–Al_2O_3 (Table 1). However, the substitution of the more active catalyst with a less active and a 6-fold decrease of the total Pd content (Fig. 4, curve 3) did not decrease the methane combustion efficiency compared to the previous test (Fig. 4, curve 2) where the total Pd content was 0.6 wt.%. Thus, increase of the efficiency of the use of the catalyst granules even at a relatively short length of the CCC results in a noticeable improvement of the overall CCC efficiency at a low total Pd loading.

However, such CCC design produced a larger pressure drop than the uniform catalyst package with ring-shaped catalysts. The pressure drop in the two-stage catalyst package was 48 mbar at GHSV = 12,500 h^{-1} and 30 mbar at GHSV = 10,000 h^{-1}. The pressure drop in the layer of the spherical Pd–Mn–La–Al_2O_3 catalyst was 20 and 13 mbar, respectively.

The tests of CCC with a combined two-stage catalyst package at lower inlet temperature showed that the inlet temperature decrease from 580 to 470 °C decreased the methane combustion efficiency. The methane conversion over the catalyst package Pd–Mn–La–Al_2O_3 (rings)/Pd–Mn–La–Al_2O_3 (spheres) decreased

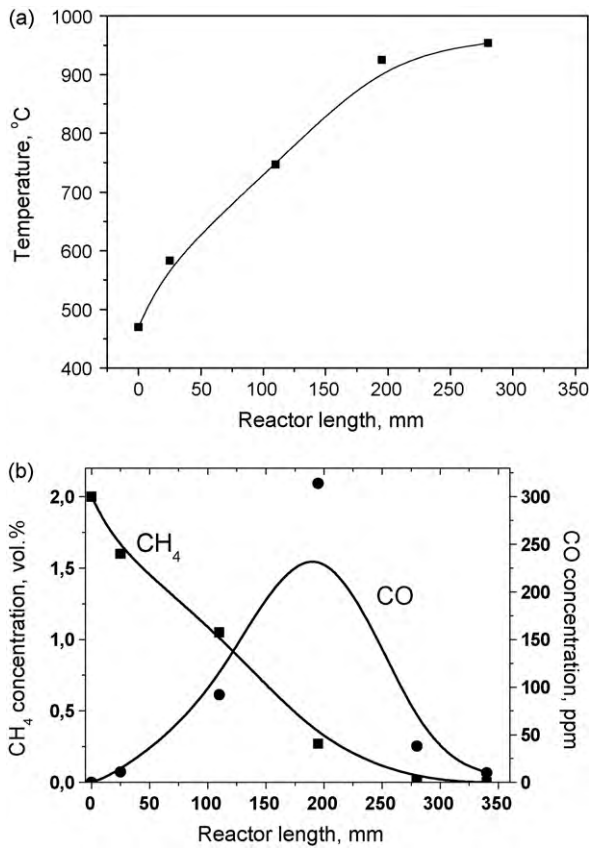

Fig. 6. Profiles of temperature (a) and methane and CO concentrations (b) along the reactor length during combustion of natural gas on a combined catalyst package Pd–Mn–La–Al_2O_3/Mn–La–Al_2O_3/Pd–Ce–Al_2O_3 (T_{in} = 470 °C, GHSV = 10,000 h^{-1}, α = 5.2).

from 99.93% to 99.7% with methane and CO concentrations 37 and 150 ppm, respectively. The methane conversion over the catalyst package Mn–La–Al_2O_3 (rings)/Pd–Mn–La–Al_2O_3 (spheres) at the inlet temperature 470 °C was only 99.4% with methane and CO concentrations 90 and 220 ppm, respectively. The increase of the methane combustion efficiency at low inlet temperature was made possible by organizing a three-stage catalyst package.

3.4. Tests of CCC with combined three-stage catalyst package

In the three-stage catalyst package we placed a highly active Pd–Ce–Al_2O_3 catalyst with 2 wt.% Pd at the entrance zone. Most of the package consisted of Mn–La–Al_2O_3 catalyst. Both catalysts were shaped as 7.5 mm × 7.5 mm × 2.5 mm rings. Pd–Mn–La–Al_2O_3 catalyst in the form of 4–5 mm spherical granules was placed in the downstream part of the catalyst package. The ratio of the catalyst layer heights was 40/240/60 mm. Similarly to the tests of two-stage packages, the ratio of the heights of ring and spherical granules was 280/60 mm. The tests were carried out at the inlet temperature 470 °C, GHSV = 10,000 h^{-1} and α = 5.2. Under such conditions the temperature at the outlet zone of the catalyst package remained at about 950 °C.

Fig. 6a shows the temperature profile along the CCC length. In the inlet zone filled with the Pd–Ce–Al_2O_3 catalyst at 25 mm from the inlet the feed is heated from 470 to 580 °C due to catalytic combustion of methane. The latter temperature is sufficiently high for effective functioning of the main Mn–La–Al_2O_3 catalyst bed. Further temperature growth from 580 to 950 °C takes place on this catalyst.

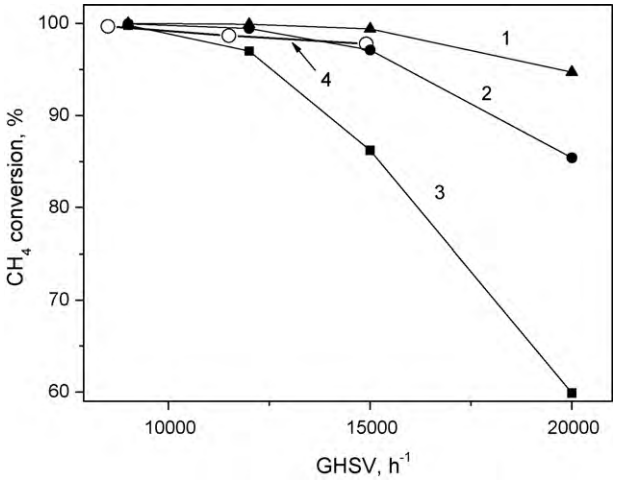

Fig. 7. Calculated dependence of methane conversion over $Mn–Al_2O_3$ catalyst (7.5 mm rings) at the initial methane concentration 1.5 vol.% on GHSV at inlet temperatures: (1) 600 °C; (2) 575 °C; 3–550 °C; (4) experimental dependence at T_{in} = 580 °C.

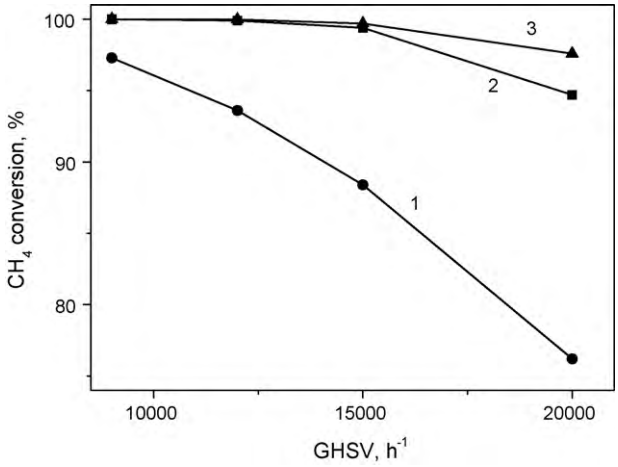

Fig. 8. Calculated dependence of methane conversion over $Mn–Al_2O_3$ catalyst on GHSV at the initial methane concentration 1.5 vol.% and T_{in} = 600 °C for catalyst granules of different sizes and shapes: (1) rings 15 mm × 15 mm × 15 mm; (2) rings 7.5 mm × 7.5 mm × 2.5 mm; (3) sphere 5 mm.

The profiles of the methane and CO concentrations along the CCC length are shown in Fig. 6b. The methane concentration profile shows a sharp concentration fall in the inlet zone where the $Pd–Ce–Al_2O_3$ catalyst is located. The main decrease of the concentration from 1.4% to 170 ppm takes place in the zone of the main catalyst $Mn–La–Al_2O_3$ (40–280 mm). Then at the CCC exit in the layer of the spherical $Pd–Mn–La–Al_2O_3$ catalyst the residual amounts of methane burn from 170 to 0–10 ppm concentrations. The concentration of the CO intermediate initially grows. Then, when most methane is oxidized, the CO concentration also decreases from 300 to 40 ppm in the $Mn–La–Al_2O_3$ bed. Finally, residual CO is burned in the spherical $Pd–Mn–La–Al_2O_3$ catalyst to 10 ppm concentrations. The pressure drop in the catalyst package was 29–30 mbar.

Thus, the use of the three-stage combined catalyst package including a thin layer of the active palladium–ceria catalyst located at the CCC entrance before the main oxide catalyst bed allows us to increase the CCC efficiency for methane combustion and obtain required low methane emission value of 10 ppm at low inlet temperature 470 °C. This additional catalyst layer provides the initial methane conversion and temperature increase before the main catalyst bed.

3.5. Comparison of calculated and experimental data on the catalyst efficiency

Fig. 7 presents the calculated dependence of methane conversion on $Mn–Al_2O_3$ (7.5 mm × 7.5 mm × 2.5 mm) catalyst on the flow rate and inlet temperature at methane concentration 1.5%. The efficiency of $Mn–La–Al_2O_3$ catalyst is described by a similar curve because the kinetic parameters of methane oxidation over these two catalysts are similar [15]. At inlet temperature 575–600 °C (Fig. 7, curves 1 and 2) high methane conversions are obtained at GHSV = 10,000 h^{-1}. Note that there is a very good correlation of the calculated data (curve 2) with the experimental results obtained under the same conditions over the $Mn–Al_2O_3$ catalyst (curve 4).

At lower temperatures of the natural gas–air mixture at the CCC inlet ≤500 °C (Fig. 7, curve 3) manganese-oxide catalysts function efficiently only at low GHSV below 10,000 h^{-1}. So, the use of a uniform layer of these catalysts is undesirable because it would require too large catalyst loading.

The results of calculations on the effect of the size and shape of catalyst granules on the efficiency of methane combustion are shown in Fig. 8. It was found that the increase of the ring diameter from 7.5 to 15 mm (Fig. 8, curves 2 and 1) resulted in a significant decrease of the combustion efficiency in good agreement with the results obtained using the large fraction of the $Mn–Al_2O_3$ catalyst (Table 3). The spherical catalyst with the granule size 5 mm (Fig. 8, curve 3) has higher methane combustion efficiency than the 7.5 mm ring catalyst.

The calculated pressure drops in the 300 mm catalyst bed during natural gas combustion at GHSV = 15,000 h^{-1} and inlet temperature 580 °C are 6, 25 and 80 mbar for 15 mm rings, 7.5 mm rings and 5 mm spheres, correspondingly. The experimental results are in good agreement with the calculations (6, 36 and 100 mbar, respectively). According to these data, the use of spherical granules in CCC is undesirable due to high pressure loss. However, the use of a thin layer of such granules can be very efficient for afterburning residual fuel and CO at the CCC outlet. Thus, based on the results of our experimental studies and mathematical calculations on the effect of granule size and shape on the parameters of the catalytic methane combustion process, the use of the catalyst shaped as 7.5 mm × 7.5 mm × 2.5 mm rings appears to be optimal for CCC of gas turbines.

The results of the mathematical calculations are in satisfactory agreement with the results of the tests. The developed approximate calculation methods can be used during development of realistic catalytic combustion chambers.

3.6. Investigation of catalysts after tests in CCC

We studied physicochemical and catalytic properties of the catalysts subjected to the tests in CCC (Table 1). For investigation we took samples from three zones of the combustion chamber at different distances from the inlet of the catalyst package: entrance zone (20–30 mm), middle zone (120–140 mm) and exit zone (200–280 mm). As the methane burning intensity was different in different zones of the catalyst package depending on the parameters of the combustion process (catalyst activity, inlet temperature, α), the temperature profile along the catalyst package changed, and the catalyst was subjected to different thermal loads. The temperature at the entrance zone was mostly 600–700 °C. In the middle zone it reached 800–900 °C, increasing further to 900–950 °C in the exit zone. Table 1 reports the characteristics of the catalysts sampled from the hottest exit zone because they reflect the most significant changes of their properties.

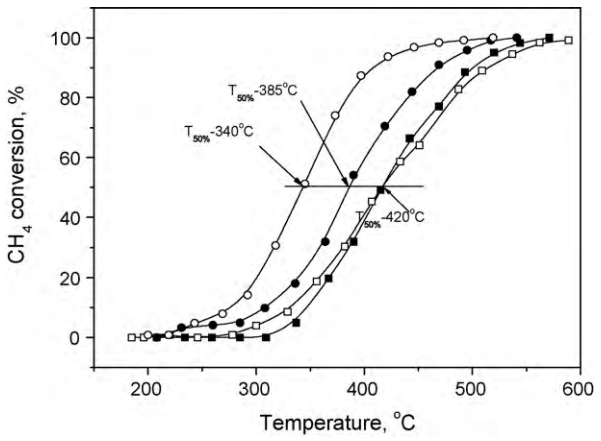

Fig. 9. Methane conversion on catalysts samples Mn–La–Al_2O_3 (■, □) and Pd–Mn–La–Al_2O_3 (●, ○): as-prepared (■, ●) and taken from the CCC hot zone after operation in tests 2 (□) and 3 (○).

Changes in the physicochemical and catalytic properties of the Mn–Al_2O_3 catalyst after 72 h on stream were observed in the samples taken from the middle and exit zones of the catalyst package. The surface area, pore volume and mechanical strength of these samples were much lower than those of the initial catalyst. According to the XRD data, the active phase of these samples Mn_2O_3 was converted to a solid solution based on (Mn, Al)Al_2O_4 spinel. Also the low-temperature alumina modification started to transform to the α-Al_2O_3 phase. The activity of the catalyst significantly decreased. The temperatures of 50% methane conversion over the samples taken from the middle and exit zones of the catalyst package were 450 and 460 °C, respectively. This is 50–60 °C higher than that of the initial catalyst. Note that the 50% methane conversion temperature equal to 450–460 °C is close to those observed over the Mn–Al_2O_3 catalysts calcined at 950 °C ($T_{50\%}$ = 435 °C) and 1000 °C ($T_{50\%}$ = 475 °C). After complete Mn_2O_3 transformation into the solid solution, the phase composition stabilized and the catalyst activity did not change in the following 250 h on stream.

Only minor changes were observed for the catalysts based on manganese–hexaaluminate (Mn–La–Al_2O_3 and Pd–Mn–La–Al_2O_3, Table 1). After 120 h of CCC tests the surface areas and pore volumes of the samples decreased by 10–20%. Minor structural changes observed for these samples consisted of the hexaaluminate phase ordering and appearance of trace amount of the α-Al_2O_3 phase in the samples taken from the middle and exit zones and originated from the effect of high temperatures on the catalysts. It was difficult to identify the PdO phase in the XRD patterns of the Pd–Mn–La–Al_2O_3 catalyst with 0.65 wt.% Pd due to overlapping of the lines attributed to the hexaaluminate phase. The catalytic characteristics of the Mn–La–Al_2O_3 catalyst did not change after the extended tests, the $T_{50\%}$ remained the same equal to 420 °C (Fig. 9). Meanwhile, the activity of the Pd–Mn–La–Al_2O_3 samples taken from the CCC hot zone even increased, the $T_{50\%}$ decreasing from 385 to 340 °C after the test (Fig. 9).

The palladium–ceria catalyst was used only in the entrance zone of the catalyst package in experiments with low T_{inlet} (470 °C). So, the temperature in the catalyst layer did not exceed 600 °C and its properties did not change (Table 1). Additional experiments on prolonged overheating of this catalyst above 750–800 °C showed that under these conditions the PdO particles were sintered to dimensions exceeding 300 Å and the catalyst partially deactivated (these data are not presented in the paper).

Thus, according to the XRD and BET data, and catalytic activity in methane oxidation the catalysts based on hexaaluminates are most thermally stable.

4. Conclusion

The catalytic combustion of natural gas over uniform and combined loadings of granulated manganese-oxide and palladium-containing catalysts was studied for optimization of the design of a catalytic package for use in CCC. The catalysts based on manganese–hexaaluminate showed high efficiency and thermal stability during combustion of natural gas for more than 120 h at the temperature in the catalyst bed as high as 950–985 °C.

Computer calculations of the catalyst efficiency depending on the reaction conditions (inlet temperature, flow rate) as well as the size and shape of granules were performed. The results of the calculations are in satisfactory agreement with the results of the experimental tests.

Granules in the form of rings with dimensions 7.5 mm × 7.5 mm × 2.5 mm were shown to be the optimal form of the catalysts. At the catalyst package height 300 mm and GHSV = 8500–15,000 h^{-1} the pressure drop in the catalyst package was lower than 40 mbar. This is less than 4% of the total pressure in CCC (1 bar). The use of 4-5 mm spherical granules in the combined loading increased the pressure drop to 48 mbar at GHSV = 12,500 h^{-1} and 30 mbar at GHSV = 10,000 h^{-1}. However, the use of a thin layer of such granules (less than 17.5%) is acceptable for afterburning residual unburned fuel and CO at the CCC exit.

The optimal design of the catalyst package for efficient combustion of lean methane-air mixture (1.5 vol.% CH_4) in CCC which is based on the obtained experimental and calculation data includes combined loading of the catalysts Mn–La–Al_2O_3 or Pd–Mn–La–Al_2O_3 (280 mm) in the form of 7.5 mm × 7.5 mm × 2.5 mm rings at the CCC inlet and Pd–Mn–La–Al_2O_3 catalyst in the forms of 4–5 mm spheres at the outlet. Such design of the catalyst package provides for the most efficient and stable natural gas combustion at the inlet temperature 570–580 °C and GHSV as high as 13,000 h^{-1} with low emission characteristics – outlet concentrations of CH_4 < 10 ppm, CO < 10 ppm, $NO_x \leq 2$ ppm.

A combined catalyst package including a 40 mm layer of an active palladium–ceria catalyst located at the CCC entrance before the main catalyst layer was shown to be efficient for natural gas combustion with similar emission characteristics and low inlet temperature 470 °C. This additional catalyst layer provides for the initial methane conversion and temperature increase before the main catalyst bed.

Acknowledgments

This study was supported by Integration projects of RAS Presidium 7.4 and 19.4, RFBR (Grants 06-08-00981 and 07-08-12272) and State Contract 02.526.12.6003.

References

[1] D.L. Trimm, Appl. Catal. 7 (1983) 249.
[2] V.N. Parmon, Z.R. Ismagilov, M.A. Kerzhentsev, in: J.T. Thomas, K.I. Zamaraev (Eds.), Perspectives in Catalysis, Chemistry for 21st Century, Monograph, Blackwell Scientific Publication, Oxford, 1992, p. 337.
[3] Z.R. Ismagilov, M.A. Kerzhentsev, Catal. Today 47 (1999) 339.
[4] L.D. Pfefferle, W.C. Pfefferle, Catal. Rev. 29 (1987) 219.
[5] R.A. Dalla Betta, J.C. Schlatter, D.K. Yee, D.G. Loffler, T. Shoji, Catal. Today 26 (1995) 329.
[6] R.A. Dalla Betta, Th. Rostrup-Nielsen, Catal. Today 47 (1999) 369.
[7] R.A. Dalla Betta, K. Tsurumi, Partial combustion catalyst of palladium on a zirconia support and a process for using it, US patent 5,405,260 (1995).
[8] R.A. Dalla Betta, M.A. Velasco, Method of thermal NOx reduction in catalytic combustion systems, US patent 6,718,772 (2002).
[9] R. Garroni, T. Griffin, J. Mantzaras, M. Reinke, Catal. Today 83 (2003) 157.
[10] J.G. McCarty, V. Wong, Catalytic combustion process, US patent 6,015,285 (2000).

[11] J.G. McCarty, M. Gusman, D.M. Lowe, D.L. Hildenbrand, K.N. Lau, Catal. Today 47 (1999) 5.
[12] L.T. Tsykoza, S.A. Yashnik, Z.R. Ismagilov, Russian Patent 2,185,238 (2002).
[13] L.T. Tsykoza, Z.R. Ismagilov, V.A. Ushakov, V.V. Kuznetsov, I.A. Ovsyannikova, Kinet. Catal. 44 (2003) 879.
[14] Z.R. Ismagilov, M.A. Kerzhentsev, V.A. Sazonov, L.T. Tsykoza, N.V. Shikina, V.V. Kuznetsov, V.A. Ushakov, S.V. Mishanin, N.G. Kozhukhar, G. Russo, O. Deutschmann, Korean J. Chem. Eng. 20 (2003) 461.
[15] Z.R. Ismagilov, N.V. Shikina, S.A. Yashnik, A.N. Zagoruiko, S.R. Khairulin, M.A. Kerzhentsev, V.N. Korotkikh, V.N. Parmon, B.I. Braynin, V.M. Zakharov, O.N. Favorski, Kinet. Catal. 49 (2008) 873.
[16] S.A. Yashnik, Z.R. Ismagilov, V.V. Kuznetsov, V.V. Ushakov, V.A. Rogov, I.A. Ovsyannikova, Catal. Today 117 (2006) 525.
[17] V.N. Parmon, Z.R. Ismagilov, O.N. Favorski, A.A. Belokon, V.M. Zakharov, Herald of the Russian Academy of Sciences, vol. 77, 2007, p. 819.
[18] O.A. Malinovskaya, V.S. Beskov, M.G. Slinko, Simulation of Catalytic Processes on Porous Grains, Nauka, Novosibirsk, 1975, p. 265 (in Russian).
[19] T. Hobler, Mass Transfer and Absorbers, Pergamon Press, Oxford, 1966.
[20] M.E. Aerov, O.M. Todes, D.A. Narinski, Apparatuses for Steady-state Granular Bed. Hydraulic and Thermal Operation Basics, Khimiya, Leningrad, 1979 (in Russian).
[21] P.G. Tsyrulnikov, V.S. Salnikov, V.A. Drozdov, S.A. Stuken, A.V. Bubnov, E.I. Grigorov, A.V. Kalinkin, V.I. Zaikovskii, Kinet. Catal. 32 (1991) 439.
[22] M. Machida, K. Eguchi, H. Arai, J. Catal. 120 (1989) 377.
[23] B.W.-L. Jang, R.M. Nelson, J.J. Spivey, M. Ocal, R. Oukaci, G. Marcelin, Catal. Today 47 (1999) 103.
[24] S. Hayashi, H. Yamada, K. Shimodaira, Catal. Today 26 (1995) 319.
[25] R.A. Dalla Betta, K. Tsurumi, Graded palladium-containing partial combustion catalyst and a process for using it, US patent 5,248,251 (1993).
[26] W. Young et al., Passively cooled catalytic combustor for a stationary combustion turbine, US patent 4,870,824 (1989).
[27] W. Pfefferle, Catalytic method, US patent 5,601,426 (1997).